Chemical Science

ROYAL SOCIETY OF CHEMISTRY

EDGE ARTICLE

View Article Online
View Journal | View Issue

Cite this: *Chem. Sci.*, 2020, **11**, 8771

All publication charges for this article have been paid for by the Royal Society of Chemistry

Intracellular monitoring of NADH release from mitochondria using a single functionalized nanowire electrode†

Hong Jiang, Yu-Ting Qi, Wen-Tao Wu, Ming-Yong Wen, Yan-Ling Liu and Wei-Hua Huang *

Mitochondria are the powerhouse of cells, and also their suicidal weapon store. Mitochondrial dysfunction can cause the opening of the mitochondrial permeability transition pore (mPTP) and nicotinamide adenine dinucleotide (NADH) release from mitochondria, eventually leading to the disruption of energy metabolism and even cell death. Hence, NADH is often considered a marker of mitochondrial function, but *in situ* monitoring of NADH release from mitochondria in single living cells remains a great challenge. Herein, we develop a functionalized single nanowire electrode (NWE) for electrochemical detection of NADH release from intracellular mitochondria by modifying conductive polymer (poly(3,4-ethylendioxythiophene), PEDOT)-coated carbon nanotubes (CNTs) on the surface of a SiC@C nanowire. The positively charged PEDOT facilitates the accumulation of negatively charged NADH at the electrode surface and CNTs promote electron transfer, thus endowing the NWE with high sensitivity and selectivity. Further studies show that resveratrol, a natural product, specifically induced NADH release from mitochondria of MCF-7 cancer cells rather than non-cancerous MCF-10 A cells, indicating the potential therapeutic effects of resveratrol in cancer treatment. This work provides an efficient method to monitor mitochondrial function by *in situ* electrochemical measurement of NADH release, which will be of great benefit for physiological and pathological studies.

Received 15th May 2020
Accepted 1st August 2020

DOI: 10.1039/d0sc02787a

rsc.li/chemical-science

Introduction

Mitochondria are critical subcellular organelles for aerobic respiration, and play central roles in cell metabolism and redox signaling.[1,2] Mitochondrial dysfunction is closely related to various human diseases, including aging, diabetes, cardiovascular diseases, neurodegenerative diseases, and cancer.[3,4] Reduced nicotinamide adenine dinucleotide (NADH) participates in some critical mitochondrial metabolic processes, such as glycolysis, tricarboxylic acid cycle and oxidative phosphorylation, and is often considered a marker indicating mitochondrial function.[5,6] Under normal physiological conditions, the mitochondrial inner membrane is impermeable to almost all metabolites, and most cellular NADH molecules are concentrated inside mitochondria and oxidized to generate ATP to maintain the mitochondrial metabolism function.[6–9] However, when cells respond to pro-apoptotic stimuli (*e.g.* reactive oxygen species and Ca^{2+} overload), the mitochondrial permeability transition pore (mPTP) opens, and allows free passage of metabolites and ions up to 1.5 kDa in size. This leads to the disruption of mitochondrial metabolism and eventually results in mitochondrial dysfunction (inner membrane potential collapse, respiratory chain uncoupling and halt of mitochondrial ATP synthesis) and cell death.[8–11] Though the opening of the mPTP and NADH release are closely involved in various diseases, this mechanism could be positively used to kill cancer cells by some anticancer drugs.[12,13] Therefore, real time and quantitative monitoring of NADH release from intracellular mitochondria can not only help to understand the dynamics of metabolism signaling and mitochondrial function, but also evaluate the potential anticancer efficacy of some drugs.

Up to now, several methods such as fluorescence, electrochemistry, enzymatic assays, capillary electrophoresis and high-performance liquid chromatography have been developed for detection of NADH.[7,14–18] Among them, electrochemical methods show unique advantages in real time monitoring with high sensitivity and a fast response. However, the oxidation of NADH at ordinary electrodes suffers from a high overpotential and surface fouling associated with the accumulation of reaction products.[19] Consequently, strategies have been developed to reduce the overpotential and minimize surface passivation effects by constructing sensing interfaces with redox mediators, carbon nanomaterials, metal complexes or conducting polymers.[19–24] The monitoring of biomolecules in single living cells is of great importance to understand the dynamics of cellular

College of Chemistry and Molecular Sciences, Wuhan University, Wuhan 430072, China. E-mail: whhuang@whu.edu.cn

† Electronic supplementary information (ESI) available. See DOI: 10.1039/d0sc02787a

functions when cells deal with environmental stresses, and some methods are constantly being developed.[25–27] Even so, *in situ* electrochemical monitoring of intracellular NADH still remains a great challenge. In this respect, nanoelectrochemical methods hold the remarkable advantage of high spatiotemporal resolution,[28–31] and have been designed for monitoring of important molecules such as neurotransmitters,[32–36] proteins[37,38] and ROS/RNS[36–43] at subcellular or intracellular levels. Regarding the measurement of intracellular NADH, exciting progress has been achieved by an asymmetric nanopore electrode-based amplification mechanism,[44] which indicates the promising potential of nanoelectrode electrochemistry in monitoring of NADH levels and their fluctuation within living cells.

We recently reported a novel kind of single SiC@C nanowire electrode (NWE) with excellent mechanical and electrochemical stability. After being platinized, these NWEs have been successfully used to monitor ROS/RNS inside single phagolysosomes of living macrophages or release from intracellular mitochondria with minimal perturbations to maintain the cell viability.[45–47] Herein, in this work, to endow the single NWEs with desired performances toward NADH measurement, we co-modified the SiC@C nanowire with a conductive polymer (poly(3,4-ethylendioxythiophene), PEDOT) and carbon nanotubes (CNTs). The positively charged PEDOT facilitates the accumulation of the negatively charged NADH at the electrode surface due to the electrostatic attraction, and CNTs promote electron-transfer reactions because of their high electrical conductivity. The as-prepared CNTs@PEDOT-NWE shows excellent electrochemical and antifouling performance, making it perfectly apt to monitor intracellular NADH in real time. With the employment of CNTs@PEDOT-NWE amperometry, the process of glucose- and resveratrol (a natural product)-induced NADH release from intracellular mitochondria was successfully investigated. This work achieved *in situ* monitoring of NADH release from mitochondria within single living cells, and provided an efficient tool for better understanding of the role of NADH in various physiological and pathological conditions.

Results and discussion

Fabrication and characterization of the CNTs@PEDOT-NWE

The single CNTs@PEDOT-NWE was prepared by modifying PEDOT-coated CNTs (CNTs@PEDOT) on a single SiC@C nanowire, and the fabrication process is illustrated in Scheme 1 and described in detail in the Experimental section. Prior to modification, negatively charged sodium carboxymethyl cellulose (CMC) was coated on the surface of a nanowire to promote the immobilization of positively charged CNTs@PEDOT. Then the modified nanowire was transferred into a glass micropipette with a liquid metal and wax seal to achieve a CNTs@PEDOT-NWE with a controllable exposed length and effective insulation. The length and the diameter of the NWE were controlled to less than 10 μm and 700 nm, respectively, which makes it easy for the NWE to be inserted into a cell without obviously influencing cell viability. Compared with the very smooth surface of the SiC@C nanowire (Fig. 1a), a polymer film and CNTs could be clearly seen on the CNTs@PEDOT-NWE (Fig. 1b). The successful preparation of the CNTs@PEDOT-NWE was further rationalized and proved by FTIR spectroscopy. The peaks located at around 1076 cm^{-1} (Fig. 1c, black line) were attributed to C–OH stretching vibrations,[48] which suggested that CMC was stably immobilized on the SiC@C nanowire by hydrogen bonding between the C–OH of the SiC@C nanowire and the –COOH of CMC. Positively charged CNTs@PEDOT were immobilized on negatively charged CMC by electrostatic attraction. The peak at 1632 cm^{-1} assigned to the C=O stretching vibrations of the –COOH groups on CNTs[49] (Fig. 1c, gray line) was observed for the CNTs@PEDOT-NWE (Fig. 1c, blue line). The characteristic peaks of PEDOT located at around 1419 cm^{-1} (C=C stretching of the thiophene ring), and 953, 876 and 619 cm^{-1} (C–S bond in the thiophene ring)[50,51] were also

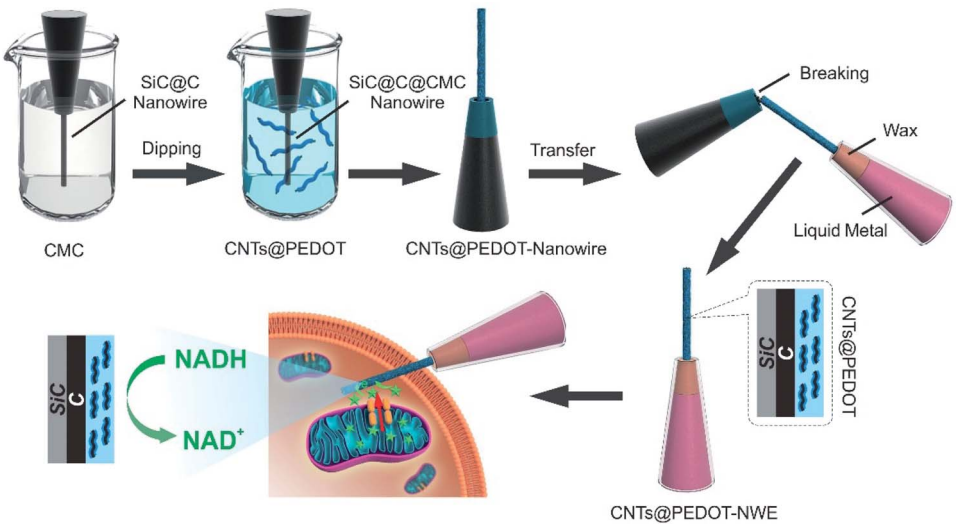

Scheme 1 Schematic diagrams showing the main fabrication processes of the CNTs@PEDOT-NWE and amperometric monitoring of NADH from intracellular mitochondria.

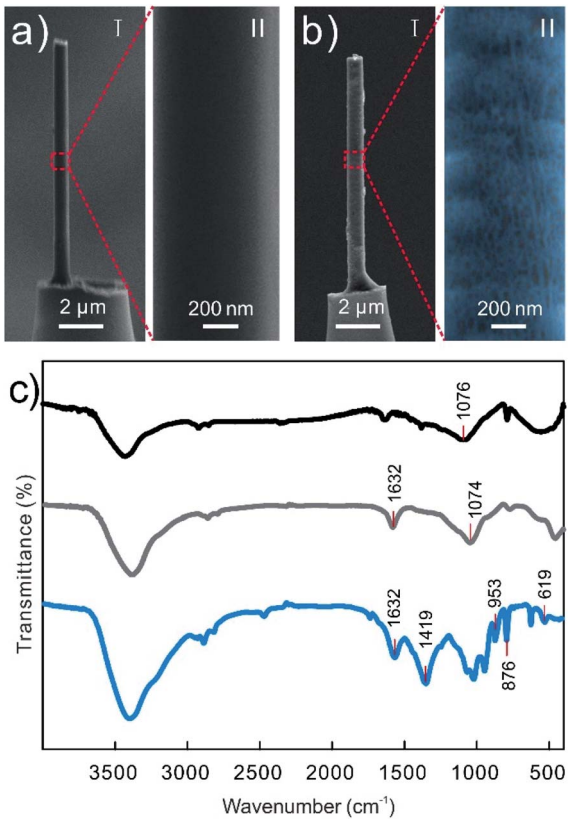

Fig. 1 (a, b) SEM images of a SiC@C-NWE (a) and CNTs@PEDOT-NWE (b). Right: An enlarged SEM image showing details of the SiC@C-NWE. To see the CNTs@PEDOT-NWE clearly, the image was pseudo-colored. (c) FTIR spectra of the SiC@C-NWE (black line), CNT–COOH (gray line) and the CNTs@PEDOT-NWE (blue line).

shown for the as-prepared NWE (Fig. 1c, blue line). These results demonstrated the successful fabrication of the single CNTs@PEDOT-NWE.

Electrochemical performance of the CNTs@PEDOT-NWE

In order to confirm the improved electrochemical responses by CNTs@PEDOT modification (the optimization of the CNTs/PEDOT ratio is shown in Fig. S1†), cyclic voltammograms (CVs) of 1 mM $Ru(NH_3)_6^{3+}$ and 2 mM NADH at the SiC@C-NWE, PEDOT-NWE and CNTs@PEDOT-NWE were examined and compared. The steady-state CVs could be obtained at all three kinds of NWEs in 1 mM $Ru(NH_3)_6^{3+}$, and compared with that of the SiC@C-NWE. The limiting diffusion currents at the PEDOT-NWE and CNTs@PEDOT-NWE were increased by 20% and 70%, respectively (Fig. 2a). This indicated the excellent electrochemical performance of the three kinds of NWEs, and the increase of the apparent electrochemical radius as well as the electroactive areas after PEDOT and CNT modification. However, the oxidation currents (at 0.8 V) of NADH at the PEDOT-NWE and CNTs@PEDOT-NWE were *ca.* 5 times and 9 times larger than that at the SiC@C-NWE, demonstrating that the electrochemical oxidation of NADH was significantly promoted (Fig. 2b). This is probably attributed to the

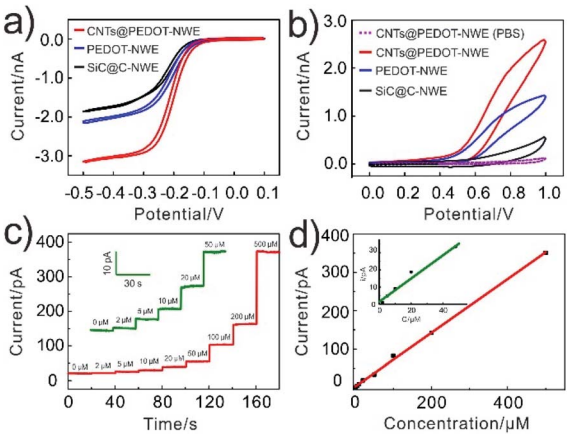

Fig. 2 Electrochemical behaviours of the CNTs@PEDOT-NWE. (a) CVs recorded at different NWEs for 1 mM $Ru(NH_3)_6^{3+}$. (b) CVs recorded for PBS without (dashed line) or with (solid line) 2 mM NADH at the NWE. (c, d) Amperometric responses of the CNTs@PEDOT-NWE poised at +0.8 V *vs.* Ag/AgCl to a series of increasing NADH concentrations (c) and the corresponding calibration curves (d).

electrostatic interaction between NADH and PEDOT and the excellent electrochemical catalytic properties of CNTs for NADH oxidation. We examined the CV responses of 8 CNTs@PEDOT-NWEs toward 2 mM NADH and found that the electrode-to-electrode variation was minimal with a relative standard deviation of 1.3% (Fig. S2†), showing good reproducibility of the fabrication and performance of the CNTs@PEDOT-NWEs.

The detection capability of the CNTs@PEDOT-NWE was further evaluated by the amperometric method, and a good linear relationship was obtained between the oxidation current and NADH concentration from 2 to 500 μM (Fig. 2c and d). The detection limit was calculated to be *ca.* 0.7 μM (S/N = 3, R^2 = 0.998), which is lower than that of classical amperometric NADH detectors (Table S1†), and is 2–3 orders of magnitude lower than the intracellular NADH level (30–800 μM).[7,52,53] The good stability of the CNTs@PEDOT-NWE was verified by negligible fluctuation of the oxidation current during successive detection of 2 mM NADH solution with the NWE for 10 days (Fig. S3†). The selectivity was also investigated, and the results indicated that the CNTs@PEDOT-NWE showed high selectivity toward NADH without obvious interference from other biomolecules (*e.g.* H_2O_2, glutathione, glucose, pyruvic acid, ATP and ADP) potentially involved in the mitochondrial metabolism, even if all the interferents were present at the same time (Fig. S4†). Furthermore, the as-prepared NWEs exhibited excellent antibiofouling properties, and the response of the CNTs@PEDOT-NWE could maintain over 98.7% (n = 4) of the original current after passivation treatment with a cell culture medium for 3 hours (Fig. S5†). This can be ascribed to the effective anti-adsorption of PEDOT and CNTs.[54,55] Taken together, the excellent sensing ability of the CNTs@PEDOT-NWE in terms of sensitivity, selectivity, stability, antifouling performance and spatial resolution demonstrates that this kind of NWE is appropriate for quantitative monitoring of intracellular NADH in real time.

Monitoring of intracellular NADH levels in MCF-7 cells under glucose and paclitaxel treatments

For intracellular monitoring, the nano-sized CNTs@PEDOT-NWE could be easily inserted into the cell membrane, and cell membranes are tightly sealed around the NWE, which could be confirmed by adding $Ru(NH_3)_6^{3+}$ into the PBS cell bath and then checking its reduction current change on the nano-electrode.[32,36,42] Since the positive Ru^{3+} complex is reducible at the electrode but cannot cross over intact cellular membranes, the limiting reduction current of $Ru(NH_3)_6^{3+}$ approximately dropped to *ca.* 75%, 50% and 25% of their primary value outside the cell when the CNTs@PEDOT-NWE was inserted into the cell with *ca.* 25%, 50% and 75% insertion, respectively (Fig. S6†). This demonstrates the tight sealing of the nanoelectrode by the cells. Then, the viability of the penetrated cells was verified by fluorescence staining with calcein-AM and propidium iodide (PI), signifying the cell viability and the integrity of the membrane. These experiments demonstrated that the CNTs@PEDOT-NWE is suitable for single cell detection (Fig. S7†).

The single CNTs@PEDOT-NWE was then inserted into MCF-7 cells (human breast cancer cell line) to evaluate their applicability for intracellular NADH detection. To demonstrate the capability of the CNTs@PEDOT-NWE for intracellular detection of NADH, an intracellular calibration experiment was performed by pre-loading 0, 200, 500, and 1000 μM NADH into the MCF-7 cells followed by intracellular electrochemical detection. We found that the charge increased with the increase of the NADH concentration, displaying a good linear relationship (Fig. S8†). The results suggested that the intracellular NADH fluctuations could be well quantified using the CNTs@PEDOT-NWE.

Glucose (1 mM) and paclitaxel (20 μM) were used to regulate the intracellular NADH levels (Fig. 3a). Glucose could increase the levels of NADH by enhancing intracellular metabolism while paclitaxel suppresses this process,[56,57] which was also verified by fluorescence colorimetric detection in starved cells using a NADH assay kit (Fig. 3b). As expected, when a CNTs@PEDOT-NWE was inserted into a starved MCF-7 cell, glucose stimulation induced an obvious amperometric signal increase (Fig. 3c, curve 1), while this could not be observed inside a cell without any treatment (Fig. 3c, curve 3). Conversely, when the cells were pre-treated with paclitaxel, no detectable amperometric signal increase was found after glucose stimulation (Fig. 3c, curve 2). The selectivity test has indicated the high selectivity of the CNTs@PEDOT-NWE toward NADH without obvious interference from other biomolecules potentially involved in the mitochondrial metabolism. Here the SiC@C-NWE was inserted into cells to exclude the other possible interference from electroactive species such as ascorbic acid (AA) and uric acid (UA), since it shows a good detection performance for AA and UA but a poor performance for NADH detection (Fig. S9a†). No detectable amperometric signal increase was found after glucose stimulation (Fig. S9b†). Further considering that the intracellular level of NADH is significantly higher than that of NADPH,[58,59] it can be seen that the signals we obtained came from the oxidation of intracellular NADH. Further converting the current signals to charge data

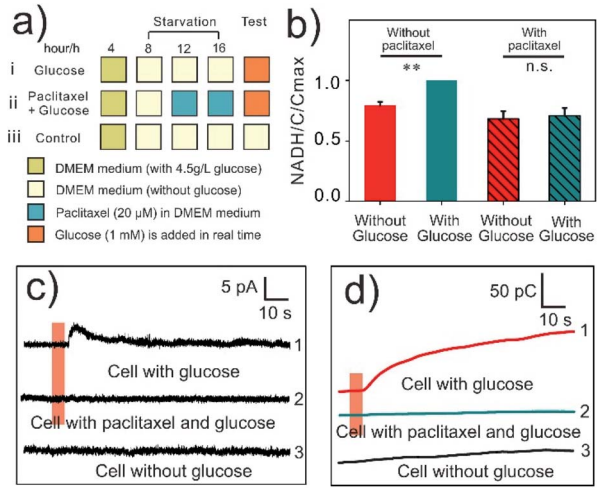

Fig. 3 (a) Experimental schedule for amperometric monitoring of intracellular NADH. (b) Intracellular levels of NADH in MCF-7 cells treated with glucose or paclitaxel + glucose (cell pre-treated paclitaxel for 4 h), and the levels of NADH were measured with a NAD^+/NADH assay kit (means and SEM, $n = 3$, $^{**}P < 0.01$). (c) Amperometric traces obtained from MCF-7 cells with 1 mM glucose injection (curve 1), 20 μM paclitaxel incubation and 1 mM glucose injection (curve 2), and without glucose injection (curve 3). (d) The charge chart of the amperometric curves under 3 kinds of detection conditions. The orange line indicates the time of glucose injection.

(the corresponding charge statistics are shown as Fig. S10†) indicated that the amount of intracellular NADH generation in glucose-induced cells was increased by an average of 8.6-fold compared with that in paclitaxel pre-treated cells, and 5.2-fold compared with that in starved cells.

After cell experiments, the electrochemical response of the CNTs@PEDOT-NWE to NADH was almost unchanged, indicating that the PEDOT and CNT modification effectively prevented the electrode surface fouling caused by intracellular biomolecules (Fig. S11†). These results demonstrated that the CNTs@PEDOT-NWE possessed the capability to quantitatively monitor NADH concentration variations inside single living cells in real time.

Resveratrol specifically triggers MCF-7 cancer cells to release NADH from mitochondria

Resveratrol (RSV) is a naturally occurring polyphenol found in grapes, red wines and other food products, and exhibits many health-promoting effects such as anti-oxidative, anti-inflammatory, and anti-proliferative properties.[60,61] In recent years, RSV has been proposed as a novel therapeutic agent for cancer treatment, but the mechanism to promote tumor cell apoptosis is not totally clear.[12,60] Some studies suggested that RSV induced cell death in tumor cells *via* mitochondrial-dependent pathways.[13,62] Herein, the RSV-induced NADH release was measured using single CNTs@PEDOT-NWEs to evaluate its effect on mitochondrial function. With the functionalized NWE inserted into a MCF-7 cell and positioned near mitochondria (Fig. 4a), an obvious increase of the amperometric signal was observed after stimulating the cell with RSV (Fig. 4b, curve 1). However, no

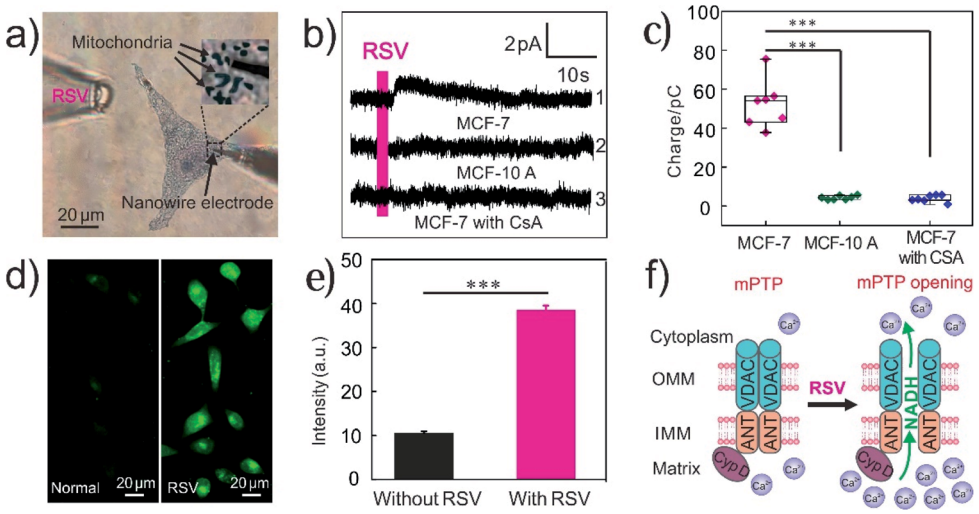

Fig. 4 (a) Bright-field photomicrograph with a 100× objective showing the living cells stained with Janus green B and the CNTs@PEDOT-NWE positioned near the mitochondria of a MCF-7 cell (insert: A 5× magnified image of box). (b) Amperometric traces obtained from a MCF-7 cell (curve 1), a MCF-10 A cell (curve 2) and a MCF-7 cell with CsA (cell pre-treated CsA for 4 h) incubation (curve 3), and (c) the corresponding charge statistics ($n = 7$, ***$P < 0.001$); the red line indicates the time of 1 mM resveratrol injection. (d) Fluorescence imaging of Ca^{2+} in MCF-7 cells before and after RSV incubation, and (e) the corresponding statistical results (means and SEM, $n = 70$, ***$P < 0.001$). (f) Schematic illustration of RSV-induced NADH release from intracellular mitochondria (mPTP is thought to consist of the voltage-dependent anion channel (VDAC) in the outer membrane, adenine nucleotide translocase (ANT) in the mitochondrial inner membrane and cyclophilin D (CypD) in the mitochondrial matrix).

detectable amperometric signal increase was found when the MCF-7 cells were pretreated with 2 μM cyclosporine A (CsA, an inhibitor to inhibit the opening of the mPTP[11]) before RSV stimulation (Fig. 4b, curve 3). This indicated that RSV probably caused the opening of the mPTP and the increase of intracellular NADH levels. The statistical results showed that the overall charge of RSV-induced NADH released from mitochondria was 52.5 ± 4.6 pC (Fig. 4c, $n = 7$). According to the Faraday law ($Z = Q/nF$, Z is the amount of substance, Q is the amount of charge, F is the Faraday constant, and n is number of electrons transferred) and volume of a MCF-7 cell (the average diameter of spherical MCF-7 cells is about 11 μm), the average increase of the intracellular NADH concentration induced by RSV was calculated to be 400 ± 32 μM. Similarly, no detectable amperometric signal increase was found after RSV stimulation when the SiC@C-NWE was inserted into a cell (Fig. S9c†).

Interestingly, RSV-induced NADH release was not found in non-cancerous MCF-10 A cells (Fig. 4b, curve 2), which suggested that RSV may specifically induce mPTP opening and NADH release in cancer cells.[62–64] This is a very exciting result but the underlying mechanism needs to be deeply investigated.

Considering that Ca^{2+} is the activator of the mPTP,[65–69] intracellular Ca^{2+} fluorescence imaging was performed. The results showed that RSV induced a four-fold increase in the intracellular Ca^{2+} concentration compared with that from the control group (Fig. 4b and e). Therefore, we speculated that resveratrol induced a large amount of Ca^{2+} to release from the endoplasmic reticulum and flow into the mitochondria to induce the opening of the mPTP, thereby promoting NADH release from mitochondria (Fig. 4f). The release of NADH from intracellular mitochondria affected mitochondrial bioenergy synthesis and thus induced mitochondria dysfunction and cancer cell apoptosis. Our results verified the antitumor properties of RSV and suggested that NADH could possibly be one of the key molecules for understanding the related pathways.

Conclusions

In summary, we prepared a functionalized nanowire electrode by a facile and versatile approach, and developed an effective strategy to quantitatively monitor intracellular NADH *in situ* inside single living cells. The glucose and RSV-induced intracellular NADH level increase was successfully monitored in real time, and we found that RSV triggered NADH release from mitochondria specifically from MCF-7 cancer cells for the first time. Though a number of experiments remained to be performed to reveal the underlying mechanism, our results provided further evidence that RSV could induce mitochondrial dysfunction in cancer cells, and thus verified the effectiveness of its promising anticancer properties in future cancer therapy. Moreover, with this CNTs@PEDOT-NWE, real-time quantification of the NADH fluctuations induced by other drugs could also be achieved. Moreover, the strategy of modifying the nanowire electrode can be further extended to nanoelectrode arrays for monitoring a large number of cells in a tissue to obtain biologically relevant statistics as well as tissue behaviors,[70] which will be of great significance for future biomedical studies and clinical evaluations.

Experimental

Materials

PEDOT:PSS (Clevios PH 1000) was purchased from Wuhan Zhuojia Technology Co., Ltd. (China). Carbon nanotubes

(SWCNTs-COOH, diameter 1–3 nm, and length 1–3 μm) were obtained from XFNANO Materials Tech Co., Ltd. (Jiangsu, China). Sodium carboxymethyl cellulose (CMC) and D (+)-glucose were bought from Aladdin Industrial Co., Ltd. (Shanghai, China). Paclitaxel was purchased from Shanghai Macklin Biochemical Co., Ltd. (China). Resveratrol and Janus green B were bought from Sigma-Aldrich (USA). Fluo-4 AM was obtained from Beyotime Biotechnology Co., Ltd. (China). Dulbecco's modified Eagle's medium (DMEM), fetal bovine serum, penicillin and streptomycin for cell culture were obtained from GIBCO (USA). All the other chemicals and solvents of analytical grade were obtained from Sinopharm Chemical Reagent Co., Ltd. (China) and used as received unless stated otherwise.

CNTs@PEDOT-NWE fabrication

Single conductive CNTs@PEDOT nanowire fabrication. To obtain a CNTs@PEDOT nanowire, a SiC@C nanowire was first fabricated *via* chemical vapor deposition according to our previously published procedure.[42] PEDOT-coated SWCNTs (CNTs@PEDOT) were obtained by mixing SWCNTs–COOH (10 mg) and PEDOT:PSS solution (containing 1% PEDOT:PSS solution with 5% DMSO) with adequate ultrasonic treatment. The SiC@C nanowire was immersed in CMC aqueous solution (10 mM) for 10 minutes, followed by drying in an oven at 75 °C. Then, the CMC-coated SiC@C nanowire was immersed in the CNTs@PEDOT solution for 10 minutes, followed by drying in an oven at 75 °C. To ensure that the SiC@C nanowire was completely coated with the CNTs@PEDOT composite, the SiC@C nanowire was repeatedly immersed in CMC aqueous solution and CNTs@PEDOT solution three times. Because of the electrostatic attraction, a SiC@C@CMC@CNTs@PEDOT nanowire (CNTs@PEDOT nanowire) was obtained.

Transfer of the CNTs@PEDOT nanowire into another micropipette to obtain a single CNTs@PEDOT-NWE. A borosilicate capillary (1B100-4, World Precision Instruments, USA) was pulled to form a glass micropipette with a tip diameter about 1–2 μm. A liquid metal was then injected into the glass micropipette and the glass micropipette tip was sealed with wax (80# Microcrystalline wax, Shuangfeng WaxCo., China). With the help of a micromanipulator, the CNTs@PEDOT nanowire was inserted into the glass micropipette after the wax melted. When the protruding length was about 10 μm, the CNTs@PEDOT nanowire was detached from the quartz micropipette. Then the heating of the wax was stopped, and the CNTs@PEDOT-NWE was successfully obtained.

FT-IR characterization of CNTs@PEDOT nanowires

The SiC@C nanowires were prepared *via* chemical vapor deposition using the fabrication conditions of the single SiC@C nanowire. The CNTs@PEDOT nanowires were prepared in solution, and the fabrication procedures are the same as that of the CNTs@PEDOT-NWE. Then, 0.3 mg SiC@C nanowires or 0.3 mg CNTs@PEDOT nanowires were dispersed in KBr discs, respectively, and characterized by Fourier transform infrared (FT-IR) spectroscopy (Nicolet-6700, Thermo Fisher).

Cell culture

MCF-7 cells were cultured in DMEM with 10% fetal bovine serum and 1% penicillin–streptomycin at 37 °C in a 5% CO_2 humidified atmosphere. Before further electrochemical experiments, the MCF-7 cells were seeded on small circular glass slides (diameter 7 mm) and cultured for 12 hours to obtain essentially isolated single cells.

Cellular NADH concentration measurements by using a NADH assay kit

The concentration of cellular NADH was measured using a NADH Assay Kit (Beyotime Biotechnology Co., Ltd, China) following the manufacturer's instructions. Briefly, MCF-7 cells were cultured and seeded in four culture dishes (diameter 15 mm, named 1#, 2#, 3# and 4#, and each one contained $\sim 1 \times 10^7$ cells). The cells of 1# and 2# were incubated in DMEM for 4 h, while 3# and 4# were cultured in DMEM containing 20 μM paclitaxel for 4 h. Then, the cells of 1# and 3# were treated with 100 mM glucose at 37 °C for 30 min. Finally, the cellular NADH concentration in the 4 dishes was extracted and quantified following the manufacturer's instructions.

Fluorescence imaging of Ca^{2+} in MCF-7 cells treated with resveratrol

The MCF-7 cells were seeded in 35 mm confocal dishes and cultured overnight. Two batches of cells were incubated without and with 10 μM resveratrol for 4 h, respectively, and then rinsed twice with PBS before adding Fluo-4 AM (2 μM in culture medium). The mixture was incubated in a 37 °C incubator for 45 min. After washing three times with PBS to remove Fluo-4 AM which did not enter the cells, fluorescence (FL) microphotographs were taken by using a charge-coupled device (CCD) mounted on an inverted fluorescence microscope (Zeiss Observer Z1, Carl Zeiss, Germany).

Bright field and fluorescence visualization of mitochondria inside the cell

For bright field visualization of the mitochondria, the living cells attached to a small circular glass slide (diameter 7 mm) were treated with 2 μM Janus green B for 20 min at 37 °C. After being washed and cultured in PBS, the cells were applied in the electrochemical experiments.

Amperometric measurements, data acquisition and analysis

All the amperometric monitoring experiments were conducted on the stage of an inverted microscope (AxioObserver Z1 fluorescence microscope, Zeiss, Germany) placed in a Faraday cage, and all the apparatuses were grounded through a common ground. The living cells were stained with Janus green B as mentioned above. The single CNTs@PEDOT-NWE was firstly placed near the cell membranes with a micromanipulator (TransferMan NK2, Eppendorf) under the microscope using a 40× objective lens, and we can see that the cell membranes were slightly deformed by the contact pressure. Then, the nanowire electrode was gently moved forward over 6 μm to

ensure insertion inside the cell and the tip near mitochondria. Finally, a constant potential of 800 mV (*vs.* Ag/AgCl wire as the reference/counter electrode) was applied to the nanowire electrode for amperometric measurements. During the experiment, the length of the CNTs@PEDOT-NWE inside the cells was precisely controlled and digitally displayed using a micromanipulator, which ensured that the insertion depth of each electrode was nearly equal. When a stable current baseline was achieved, by using another micromanipulator, 1 mM glucose or resveratrol solution was delivered *via* a glass capillary which was connected to an injection pump and placed about 50 μm away from the cell.

The current transients were recorded with a patch-clamp amplifier (EPC-10, HEKA Electronics, Germany) in a 2-electrode electrochemical mode at a constant potential of 800 mV *vs.* Ag/AgCl wire as the reference/counter electrode. Signals were sampled at 10 kHz, and Bessel filtered at 2.9 kHz. Raw amperometric data were collected using "Pulse" software, and analyzed by using Origin Pro 9.0 Data Analysis and Graphing Software.

Conflicts of interest

There are no conflicts to declare.

Acknowledgements

This work was supported by the National Natural Science Foundation of China (Grants 21675121, 21725504, and 21721005).

References

1 J. R. Friedman and J. Nunnari, *Nature*, 2014, **505**, 335–343.
2 L. Galluzzi, O. Kepp and G. Kroemer, *Nat. Rev. Mol. Cell Biol.*, 2012, **13**, 780–788.
3 J. Nunnari and A. Suomalainen, *Cell*, 2012, **148**, 1145–1159.
4 D. C. Chan, *Cell*, 2006, **125**, 1241–1252.
5 A. Mayevsky and E. Barbiro-Michaely, *Int. J. Biochem. Cell Biol.*, 2009, **41**, 1977–1988.
6 Y. Zhao and Y. Yang, *Free Radical Biol. Med.*, 2016, **100**, 43–52.
7 Y. Zhao, J. Jin, Q. Hu, H. Zhou, J. Yi, Z. Yu, L. Xu, X. Wang, Y. Yang and J. Loscalzo, *Cell Metab.*, 2011, **14**, 555–566.
8 L. R. Stein and S. Imai, *Trends Endocrinol. Metab.*, 2012, **23**, 420–428.
9 L. Soane, S. Kahraman, T. Kristian and G. Fiskum, *J. Neurosci. Res.*, 2007, **85**, 3407–3415.
10 N. Zamzami and G. Kroemer, *Nat. Rev. Mol. Cell Biol.*, 2001, **2**, 67–71.
11 J. F. Dumas, L. Argaud, C. Cottet-Rousselle, G. Vial, C. Gonzalez, D. Detaille, X. Leverve and E. Fontaine, *J. Biol. Chem.*, 2009, **284**, 15117–15125.
12 S. Fulda, L. Galluzzi and G. Kroemer, *Nat. Rev. Drug Discovery*, 2010, **9**, 447–464.
13 M. Naoi, Y. Wu, M. Shamoto-Nagai and W. Maruyama, *Int. J. of Mol. Sci.*, 2019, **20**, 2451–2482.
14 E. Suraniti, V. S. Vajrala, B. Goudeau, S. P. Bottari, M. Rigoulet, A. Devin, N. Sojic and S. Arbault, *Anal. Chem.*, 2013, **85**, 5146–5152.
15 G. H. Patterson, S. M. Knobel, P. Arkhammar, O. Thastrup and D. W. Piston, *Proc. Natl. Acad. Sci. U. S. A.*, 2000, **97**, 5203–5207.
16 Q. Zhang, D. W. Piston and R. H. Goodman, *Science*, 2002, **295**, 1895–1897.
17 W. Xie, A. Xu and E. S. Yeung, *Anal. Chem.*, 2009, **81**, 1280–1284.
18 H. Yang, T. Yang, J. A. Baur, E. Perez, T. Matsui, J. J. Carmona, D. W. Lamming, N. C. Souza-Pinto, V. A. Bohr, A. Rosenzweig, R. de Cabo, A. A. Sauve and D. A. Sinclair, *Cell*, 2007, **130**, 1095–1107.
19 F. S. Omar, N. Duraisamy, K. Ramesh and S. Ramesh, *Biosens. Bioelectron.*, 2016, **79**, 763–775.
20 L. Zhao, R. Qian, W. Ma, H. Tian and Y. Long, *Anal. Chem.*, 2016, **88**, 8375–8379.
21 M. Wooten and W. Gorski, *Anal. Chem.*, 2010, **82**, 1299–1304.
22 J. M. Goran, C. A. Favela and K. J. Stevenson, *Anal. Chem.*, 2013, **85**, 9135–9141.
23 H. Teymourian, A. Salimi and R. Hallaj, *Biosens. Bioelectron.*, 2012, **33**, 60–68.
24 L. Meng, A. P. F. Turner and W. C. Mak, *Biosens. Bioelectron.*, 2018, **120**, 115–121.
25 A. Fulati, S. M. U. Ali, M. H. Asif, N. U. H. Alvi, M. Willander, C. Brannmark, P. Stralfors, S. I. Borjesson, F. Elinder and B. Danielsson, *Sens. Actuators, B*, 2010, **150**, 673–680.
26 F. B. Meng, J. H. Yang, T. Liu, X. L. Zhu and G. X. Li, *Anal. Chem.*, 2009, **81**, 9168–9171.
27 F. J. Rawson, C. L. Yeung, S. K. Jackson and P. M. Mendes, *Nano Lett.*, 2012, **13**, 1–8.
28 C. Amatore, S. Arbault, M. Guille and F. Lemaitre, *Chem. Rev.*, 2008, **108**, 2585–2621.
29 J. Clausmeyer and W. Schuhmann, *TrAC, Trends Anal. Chem.*, 2016, **79**, 46–60.
30 Y. L. Ying, Z. Ding, D. Zhan and Y. T. Long, *Chem. Sci.*, 2017, **8**, 3338–3348.
31 P. E. Oomen, M. A. Aref, I. Kaya, N. T. N. Phan and A. G. Ewing, *Anal. Chem.*, 2018, **91**, 588–621.
32 Y. T. Li, S. H. Zhang, L. Wang, R. R. Xiao, W. Liu, X. W. Zhang, Z. Zhou, C. Amatore and W. H. Huang, *Angew. Chem., Int. Ed.*, 2014, **53**, 12456–12460.
33 Y. T. Li, S. H. Zhang, X. Y. Wang, X. W. Zhang, A. I. Oleinick, I. Svir, C. Amatore and W. H. Huang, *Angew. Chem., Int. Ed.*, 2015, **54**, 9313–9318.
34 Y. Tang, X. K. Yang, X. W. Zhang, W. T. Wu, F. L. Zhang, H. Jiang, Y. L. Liu, C. Amatore and W. H. Huang, *Chem. Sci.*, 2020, **11**, 778–785.
35 X. Li, S. Majdi, J. Dunevall, H. Fathali and A. G. Ewing, *Angew. Chem., Int. Ed.*, 2015, **54**, 11978–11982.
36 W. Zhu, C. Gu, J. Dunevall, L. Ren, X. Zhou and A. G. Ewing, *Angew. Chem., Int. Ed.*, 2019, **131**, 4282–4286.
37 R. R. Pan, M. C. Xu, D. C. Jiang, J. D. Burgess and H. Y. Chen, *Proc. Natl. Acad. Sci. U. S. A.*, 2016, **113**, 11436–11440.
38 R. R. Pan, M. C. Xu, J. D. Burgess, D. C. Jiang and H. Y. Chen, *Proc. Natl. Acad. Sci. U. S. A.*, 2018, **115**, 4087–4092.

39 Y. Wang, J. M. Noel, J. Velmurugan, W. Nogala, M. V. Mirkin, C. Lu, M. G. Collignon, F. Lemaitre and C. Amatore, *Proc. Natl. Acad. Sci. U. S. A.*, 2012, **109**, 11534–11539.
40 Y. Li, K. Hu, Y. Yu, S. A. Rotenberg, C. Amatore and M. V. Mirkin, *J. Am. Chem. Soc.*, 2017, **139**, 13055–13062.
41 K. Hu, Y. Li, S. A. Rotenberg, C. Amatore and M. V. Mirkin, *J. Am. Chem. Soc.*, 2019, **141**, 4564–4568.
42 J. Song, C. Xu, S. Huang, W. Lei, Y. Ruan, H. Lu, W. Zhao, J. Xu and H. Chen, *Angew. Chem., Int. Ed.*, 2018, **130**, 13410–13414.
43 X. T. Zheng, W. Hu, H. Wang, H. Yang, W. Zhou and C. M. Li, *Biosens. Bioelectron.*, 2011, **26**, 4484–4490.
44 Y. L. Ying, Y. X. Hu, R. Gao, R. J. Yu, Z. Gu, L. P. Lee and Y. T. Long, *J. Am. Chem. Soc.*, 2018, **140**, 5385–5392.
45 X. W. Zhang, Q. F. Qiu, H. Jiang, F. L. Zhang, Y. L. Liu, C. Amatore and W. H. Huang, *Angew. Chem., Int. Ed.*, 2017, **56**, 12997–13000.
46 X. W. Zhang, A. Oleinick, H. Jiang, Q. L. Liao, Q. F. Qiu, I. Svir, Y. L. Liu, C. Amatore and W. H. Huang, *Angew. Chem., Int. Ed.*, 2019, **58**, 7753–7756.
47 H. Jiang, X. W. Zhang, Q. L. Liao, W. T. Wu, Y. L. Liu and W. H. Huang, *Small*, 2019, **15**, 1901787.
48 J. Yu, M. Gu, C. Bian, X. Xu and T. B. Tang, *Carbon*, 2013, **61**, 367–372.
49 Y. Sun, W. Huang, Y. Lin, K. Fu, A. Kitaygorodskiy, L. A. Riddle, Y. J. Yu and D. L. Carroll, *Chem. Mater.*, 2001, **13**, 2864–2869.
50 J. W. Choi, M. G. Han, S. Y. Kim, S. G. Oh and S. S. Im, *Synth. Met.*, 2004, **141**, 293–299.
51 J. Wang, B. Fang, K. Chou, C. Chen and Y. Gu, *Enzyme Microb. Technol.*, 2014, **54**, 45–50.
52 W. Ying, *Antioxid. Redox Signaling*, 2008, **10**, 179–206.
53 W. Xie, A. Xu and E. S. Yeung, *Anal. Chem.*, 2009, **81**, 1280–1284.
54 X. M. Liu, T. F. Xiao, F. Wu, M. Y. Shen, M. N Zhang, H. H. Yu and L. Q. Mao, *Angew. Chem., Int. Ed.*, 2017, **129**, 11964–11968.
55 Y. L. Liu, Y. Chen, W. T. Fan, P. Cao, J. Yan, X. Z. Zhao, W. G. Dong and W. H. Huang, *Angew. Chem., Int. Ed.*, 2020, **59**, 4075–4081.
56 L. Wang, J. Zhang, B. Kim, J. Peng, S. N. Berry, Y. Ni, D. Su, J. Lee, L. Yuan and Y. Chang, *J. Am. Chem. Soc.*, 2016, **138**, 10394–10397.
57 R. Freeman, R. Gill, I. Shweky, M. Kotler, U. Banin and I. Willner, *Angew. Chem., Int. Ed.*, 2009, **121**, 315–319.
58 W. Ying, *Antioxid. Redox Signaling*, 2008, **10**, 179–206.
59 J. P. Fessel and W. M. Oldham, *Antioxid. Redox Signaling*, 2018, **28**, 180–212.
60 M. Jang, L. Cai, G. O. Udeani, K. V. Slowing, C. F. Thomas, W. W. B. Christopher, H. S. F. Harry, N. R. Farnsworth, A. D. Kinghorn, R. G. Mehta, R. C. Moon and J. M. Pezzuto, *Science*, 1997, **275**, 218–220.
61 M. H. Keylor, B. S. Matsuura and C. R. J. Stephenson, *Chem. Rev.*, 2015, **115**, 8976–9027.
62 J. R. Gledhill, M. G. Montgomery, G. W. L. Andrew and J. E. Walker, *Proc. Natl. Acad. Sci. U. S. A.*, 2007, **104**, 13632–13637.
63 M. V. Clement, J. L. Johnson, S. H. Chawdhury and S. Pervaiz, *Blood*, 1998, **92**, 996–1002.
64 R. Peruzzo and I. Szabo, *Cancers*, 2019, **11**, 761–783.
65 T. Nakagawa, S. Shimizu, T. Watanabe, O. Yamaguchi, K. Otsu, H. Yamagata, H. Inohara, T. Kubo and Y. Tsujimoto, *Nature*, 2005, **434**, 652–662.
66 D. D. Newmeyer and S. Ferguson-Miller, *Cell*, 2003, **112**, 481–490.
67 S. Park, F. Ahmad, A. Philp, K. Baar, T. Williams, H. Luo, H. Ke, H. Rehmann, R. Taussig, A. L. Brown, M. K. Kim, M. A. Beaven, A. B. Burgin, V. Manganiello and J. H. Chung, *Cell*, 2012, **148**, 421–433.
68 P. R. van Ginkel, M. B. Yan, S. Bhattacharya, A. S. Polans and J. D. Kenealey, *Toxicol. Appl. Pharmacol.*, 2015, **288**, 453–462.
69 G. Paradies, V. Paradies, F. M. Ruggiero and G. Petrosillo, *Cells*, 2019, **8**, 728–749.
70 J. Abbott, T. Ye, K. Krenek, R. S. Gertner, S. Ban, Y. Kim, L. Qin, W. Wu, H. Park and D. Ham, *Nat. Biomed. Eng.*, 2020, **4**, 232–241.